Thermofluiddynamic pre-design of a primary surface heat exchanger under the influence of heat radiation using 1D/3D coupled simulation method

Dipl.-Ing. Tianxiao Xie, M.Sc. Tommy Starick, M.Sc. Anatol Mosgow
(Brandenburg University of Technology Cottbus-Senftenberg, Germany)

Prof. Dr.-Ing. Heinz Peter Berg, Prof. Dr.-Ing. Klaus Höschler, Prof. Dr.-Ing Heiko Schmidt
(Brandenburg University of Technology Cottbus-Senftenberg, Germany)

Abstract

Within the Framework of the "TurboFuelCell (TFC)" a highly integrated and compact energy conversion system based on Micro Gas Turbine Solid Oxide Fuel Cell (MGT-SOFC) hybrid process is being developed by the team at BTU-Cottbus Senftenberg. This work focuses on the extension of the pre-design process of a primary surface heat exchanger (PSHX), which is a key component for the coupling between MGT and SOFC, using an 1D/3D hybrid simulation method for the understanding of its behaviour under the influence of heat radiation. In a MGT-SOFC hybrid process the high temperature heat exchanger plays an important role in preheating the fresh air to a minimum operation temperature necessary for SOFC. Due to the special location of this PSHX in the TFC, it is constantly exposed to heat radiation from the SOFC module, which requires additional consideration of its influence for better model accuracy. A first design, which is later extended through an 1D Flow network model, based on $\epsilon - NTU$ method is presented. A complete 3D-CFD simulation with consideration of heat radiation is initially employed for the whole flow process to examine the first design. However, this approach proves to be highly computationally expensive due to the large dimensional difference between the plenum for cathode exhaust air and the fine channels in the PSHX. To reduce the computational effort, the flow and heat transfer in the PSHX is modelled by 1D elements. The flow in the plenum is simulated by 3D-CFD, which better accounts for convection and thermal radiation. A comparison between 3D-CFD and 1D/3D hybrid model is performed. A significant reduction of simulation time and computing resources can be achieved for well calibrated hybrid model without compromising on accuracy. In the talk, the effect of insulation layer thickness variations on the heat transfer on the plenum side due to heat radiation and their influence on the heat exchanger efficiency are discussed. Consequently, design improvements are realized based on the previous findings. Finally, the 1D/3D hybrid simulation method is evaluated and prepared for the general applications in thermal management of machines based on coupled MGT-SOFC process.

1. Introduction

The "Turbo Fuel Cell (TFC)" in development by the team at BTU Cottbus-Senftenberg is a highly integrated and compact energy conversion system [1] based on a Micro Gas Turbine Solid Oxide Fuel Cell (MGT-SOFC) cycle [2]. MGT-SOFC, with its world-record efficiency [3], offers the possibility of distributed power supply and enables higher system dynamics. MGT-SOFC, together with the "Power To X" concept, can be operated with climate-neutral hydrocarbons. The PSHX developed in this work is a key component to realize the MGT and SOFC coupling. The main function of this high temperature heat exchanger is preheating the fresh incoming air to a minimum temperature required for the SOFC.

The PSHX concept with counterflow design is chosen for easier manufacturing of this high temperature heat exchanger. The cold and hot sides are separated by a thin folded sheet, which together with the heat exchanger’s outer shell forms a single channel with a triangular cross-section on each side (Fig (1b)).

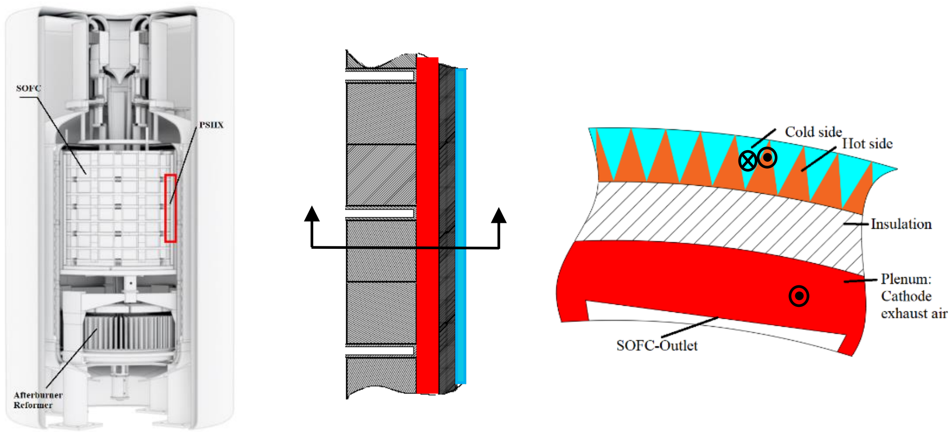

(a) (b) (c)

Figure 1: Illustrative representation of the geometry to be investigated

Since this high temperature heat exchanger is located quite close to the SOFC module (Fig. (1a) and (1b)), the hot side of PSHX together with insulation layer is constantly exposed to thermal radiation and is in contact with the hot cathode exhaust air. Characterizing this heat exchanger without considering additional heat input from thermal radiation and convection could result in inaccurate predictions of the heat exchanger output temperature. One solution is to use a full 3D simulation of Conjugate Heat Transfer (CHT) capable of capturing complicated radiation behaviour in the plenum. This requires significant computational effort because PSHX flow channels need high resolution. In contrast, a 1D/3D hybrid simulation method [5] describing the flow behaviour by certain hydraulic and thermal characteristics is more suitable. This hybrid simulation method is applied in thermal management because it can describe highly complex problems. The work of H. Jordaan et al [6] studies a shell and tube heat exchanger using a 1D/3D hybrid simulation method by modeling the flow in tubes with 1D elements and simulating that on the shell side by 3D-CFD. In the thermal management of motor vehicle, this coupled simulation is also widely adopted, e.g. coupling between 3D simulation in passenger compartment and 1D modeled cooling circuit [7], thermal management in vehicle underhood environment [8, 9], and also in engine cooling, where e.g. engine structure is described by 3D FEM and cooling circuit described by 1D Flow Network Model (FNM) [10]. In turbine blade cooling [11] the flow in cooling channels can be represented by their thermal and hydraulic characteristics in 1D elements, which has been investigated in detail using experiment or 3D-CFD and is available in many literatures or textbooks. In an electrical equipment’s thermal management this method is also massively employed [12]. The biggest advantage of the hybrid simulation besides the reduction of the computational effort for a steady-state calculation, is the characterization of transient and dynamic behavior of an extremely complicated system like the temperature oscillation of a certain structure for thermal fatigue analysis [13].

The current work presents the pre-design of an innovative PSHX based on classical heat exchanger theories and its 1D model construction in Flownex. This constructed 1D model of the heat exchanger is then coupled with a 3D model for the plenum and insulation plate. For comparison, a full 3D CHT is also performed to verify the validity and accuracy of this hybrid method. This 1D/3D hybrid method can be used to vary the plenum width and insulation thickness for quantification of heat radiation influence from the SOFC module on the heat exchanger in different configurations, so that further useful design strategies can be developed.

2. Pre-design of primary surface heat exchanger

2.1 Heat exchanger theory

A heat exchanger consists of a heat transfer process with three sub-processes: convection on both sides and heat conduction through the

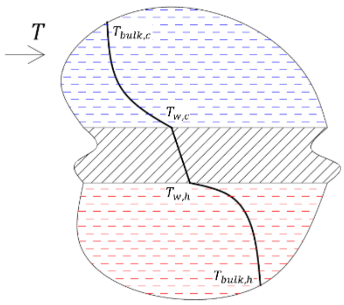

Figure 2: Temperature profile in the heat transfer process

partition wall as shown in Fig. (2). The three sub-processes are described by three corresponding thermal resistances, the sum of which is the total thermal resistance:

$$R_t = R_c + R_h + R_w; R_c = \frac{1}{\eta_c A_c \alpha_c}; R_h = \frac{1}{\eta_h A_h \alpha_h} \tag{1}$$

where R_w is the thermal resistance through heat conduction, η the fin efficiency, A the total heat surface and α the heat transfer coefficient. Subscripts c and h stand for cold and hot side respectively.

There are several methods available to design a heat exchanger, e.g., $F - LMTD$, $P - NTU$, $\epsilon - NTU$ method etc [14]. The design in this work employs the $\epsilon - NTU$ method. This method is often used, because of the clear physical meaning of the parameters occurring in this method. ϵ is a ratio between the exchanged and maximum exchangeable heat amount:

$$\epsilon = \frac{q}{q_{max}} = \frac{C_c(T_{c,o} - T_{c,i})}{C_{min}(T_{h,i} - T_{c,i})} = \frac{C_h(T_{h,i} - T_{h,o})}{C_{min}(T_{h,i} - T_{c,i})} \tag{2}$$

where $C_c = \left(\dot{m}C_p\right)_c$, $C_h = \left(\dot{m}C_p\right)_h$ and $C_{min} = \min\left(C_c, C_h\right)$. $T_{h,i} - T_{c,i}$ is the biggest temperature change that could occur in a heat exchanger. After determining ϵ, the actual amount of exchanged heat is calculated by:

$$q = \epsilon C_{min}(T_{h,i} - T_{c,i}) \tag{3}$$

NTU is a dimensionless parameter characterizing the heat transfer process. Its definition is:

$$NTU = \frac{UA}{C_{min}} \tag{4}$$

Every flow configuration (e.g., counterflow, crossflow, or parallel flow, etc.), has a unique relationship between ϵ and NTU. For performance calculation, the corresponding NTU used to determine the effectiveness according to the $\epsilon - NTU$ relationship, is determined from the inlet boundary conditions and material values. For a non-existent heat exchanger design, the process works in reverse. For example, the $\epsilon - NTU$ relationships for counterflow, parallel flow and crossflow design are presented in the Table (1) [14].

Table 1: The Relationship between ϵ and NTU for different flow type

Parallel flow		$\epsilon = \frac{1-\exp[-NTU(1+C_r)]}{1+C_r}$
Counter flow		$\epsilon = \frac{1-\exp[-NTU(1-C_r)]}{1-C_r\exp[-NTU(1-C_r)]}$ for $C_r < 1$
		$\epsilon = \frac{NTU}{1+NTU}$ for $C_r = 1$
Crossflow	Both fluids mixed	$\epsilon = 1 - \exp[(\frac{1}{C_r})(NTU)^{0.22}\{\exp[-C_r(NTU)^{0.78}] - 1\}]$
	C_{max} (mixed), C_{min} (unmixed)	$\epsilon = (\frac{1}{C_r})(1 - \exp\{-C_r[1 - \exp(-NTU)]\})$
	C_{max} (unmixed), C_{min} (mixed)	$\epsilon = 1 - \exp(-C_r^{-1}\{1 - \exp[-C_r(NTU)]\})$

2.2 Configuration of PSHX and the thermofluiddynamic design

The requirements of this heat exchanger and the respective boundary conditions are listed in Table (2). The pressure drop is not specified initially but needs to be kept as small as possible to not influence system’s overall performance negatively. Since the SOFC module has a circular design as shown in figure (1a), the high temperature heat exchanger is also designed as an annular structure with respect to the integration and compactness. Here, two

Table 2: Boundary conditions for the pre-design

Mass flow of cold side ($\dot{m}_c$) in Kg/s	0.139875
Mass flow of hot side ($\dot{m}_h$) in Kg/s	0.130875
Inlet temperature of cold side ($T_{c,i}$) in °C	571
Inlet temperature of hot side ($T_{h,i}$) in °C	831
Target outlet temperature of cold side ($T_{c,o}$) in °C	700
Target outlet temperature of hot side ($T_{h,o}$) in °C	694
Operation pressure in bar	4.6

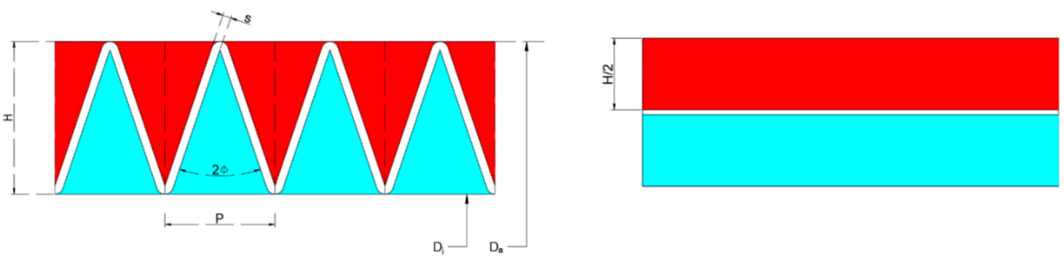

(a) Primary surface heat exchanger with triangular folded heating surface

(b) Primary surface heat exchanger with cylinder heating surface

Figure 3: Two possible heat exchanger concepts

concepts of the partition wall are considered as in Fig. (3), a cylindrical wall and a folded wall. The variant with the cylinder wall (Fig. (3b)) as a partition would provide sufficient NTU from a thermofluiddyamic perspective, if the half channel height ($\frac{H}{2}$) is small enough (theoretically smaller than 10 mm). Practically, this variant imposes many problems with thermal deformation at high temperature. The variant with folded partition wall is the focus of this work. During designing, the arc between two peaks is approximated as a straight line because the pitch is very small compared to the whole circle's circumferential length. The integer number of the pitch N is provided for avoiding fractional pitch number caused by a pitch width specification. The triangular channel is uniquely defined by the parameters used in Fig. (3a). The flow area on both sides result from the following relations:

$$A_c = N \cdot \frac{1}{2}(P_c - s)(H - s) \tag{5}$$

$$A_h = N \cdot \frac{1}{2}(P_h - s)(H - s) \tag{6}$$

The triangular channel's hydraulic diameter is determined by the following equation:

$$d_{h,c} = \frac{2(P_c - s)(H - s)}{2\sqrt{\left(\frac{P_c}{2}\right)^2 + (H-s)^2} + (P_c - s)}\ ;\ d_{h,h} = \frac{2(P_h - s)(H - s)}{2\sqrt{\left(\frac{P_h}{2}\right)^2 + (H-s)^2} + (P_h - s)} \tag{7}$$

The heating surface between the cold and hot side is as follows, assuming of identical side lengths of the triangular from both sides:

$$A_F = N \cdot 2L\sqrt{\left(\frac{P_c}{2}\right)^2 + (H - s)^2} \tag{8}$$

The definition of Reynolds number is derived from the following equation:

$$Re = \frac{\rho_m w_m d_h}{\mu_m} = \frac{\dot{m}_h d_h}{\mu_m A} \tag{9}$$

where the material properties determined by mean temperature of the respective side, which is $\frac{T_{c,i}+T_{c,o}}{2}$ for the cold side and $\frac{T_{h,i}+T_{h,o}}{2}$ for the hot side. For the design, a Reynolds number in the transition region is intentionally avoided because of difficulties in capturing the thermofluiddynamic characteristics and a higher sensitivity of the heat exchanger to disturbances [15]. Few possible combinations of geometrical parameters are considered for a rough estimation of the Reynolds number (here as an example for that of the cold side).

Table 3: Examination of Reynolds number for a few possible configurations

D_a (mm)	D_i (mm)	H (mm)	P_c (mm)	s (mm)	N (-)	Re_c (-)
0.472	0.442	15	6.86	1	200	2327
0.472	0.442	15	6.86	0.5	200	2087
0.472	0.432	20	6.79	1	200	1834
0.472	0.432	20	6.79	0.5	200	1652
0.472	0.432	20	6.79	0.2	200	1557

From Table (3), it is deducible that this heat exchanger will not work in the completely turbulent state for given rational configurations, because of a low air flow rate. According to literature, the critical Reynolds number for the duct with triangular cross-section is smaller than that for the duct with circular cross-section ($Re \approx 2300$). The transition in the duct with triangular cross-section could start already at a Reynolds number of 1700. Consequently, for this design a total channel height (H) not smaller than 20 mm and a plate thickness of about 0.1 to 0.5 mm is chosen to ensure laminar flow in the heat exchanger. For laminar flow in a triangular duct, the Nusselt number (Nu) depends only on the geometry [16].

$$Nu = \frac{\alpha d_h}{\lambda} \tag{10}$$

the heat transfer coefficient is determined for NTU calculation. This calculates the effectiveness of the heat exchanger using the $\epsilon - NTU$ relationship. For example, three possible geometrical combinations are shown in Table (4).

Table 4: Three different designs based on $\epsilon - NTU$ Theory

Channel height (H) in mm	20	20	25
Partition wall thickness (s) in mm	0.5	0.2	0.2
Pitch (P) in mm	7.07	7.14	7.71
Number of Pitches (N)	192	190	174
Total length (L) in m	1.5055	1.5055	1.5055
Outside diameter (D_a) in m	0.472	0.472	0.472
Inside diameter (D_i) in m	0.432	0.432	0.422
Nusselt number (Nu)	2.65427	2.65684	2.61823
Reynolds number of the cold side (Re_c)	1704	1622	1446
Reynolds number of the hot side (Re_h)	1429	1366	1215
Heat transfer coefficient of cold side (α_c) in W/(m^{2}K)	28.1997	27.9091	24.8632
Heat transfer coefficient of hot side (α_h) in W/(m^{2}K)	27.5254	27.2404	23.77
Total heat transfer surface (A_F) in m^2	11.46	11.51	13.15
Heat exchanger effectiveness (ϵ)	0.524	0.522	0.524
The realized NTU	1.07	1.06	1.07
Calculated outlet temperature of cold side ($T_{c,o}$) in °C	700.29	699.93	700.38

3. Methodology of the coupled simulation

A coupled simulation is understood as a simulation using different solvers for exclusively modeling or simulating part of the Multiphysics. In many situations, the physical models consist of several sub-models of distinct complexities, e.g. considering temperature control in the passenger compartment of the motor vehicle with connected cooling circuits. In this situation, the 3D flow structures in the passenger compartment are relevant, while the flow details in the cooling circuit are insignificant. Another reason for a 1D/3D co-simulation is because the transient or dynamic behaviour of a complex physical system can be analysed with acceptable computational effort.

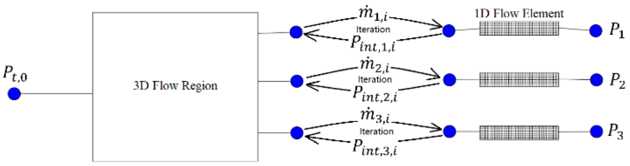

Figure 4: Hydraulic coupling between a 3D flow region and 1D flow elements

There are two typical types of coupling: thermal and hydraulic coupling. Thermal coupling concerns convection on the surface of a structure. For example, Fig. (5) shows a thermal coupling between 1D flow elements and a 3D structure. Such an approach (replacement of 3D flow by 1D flow network model) benefits transient and dynamic analysis, where enormous computational effort is associated with transient 3D flow calculation. In hydraulic coupling the 1D and 3D elements are hydraulically connected (Fig. (4)).

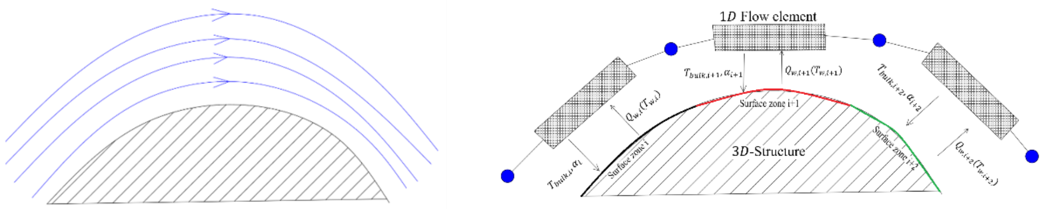

(a) Flow aver a solid body

(b) Hybrid physical model of the situation on the left

Figure 5: Illustration of a hybrid physical model of the heat convection

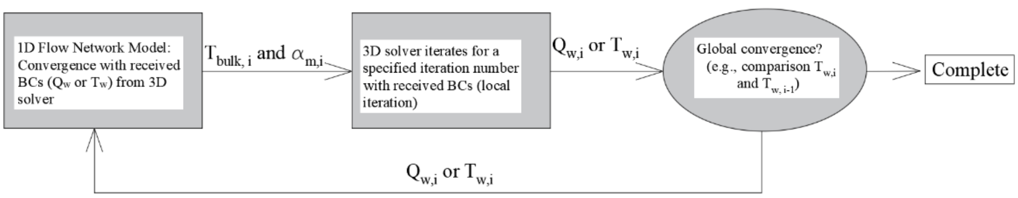

Figure 6: Iteration process of the thermal coupling

The iteration process of the thermal coupling can be found in Fig. (6). A 1D network is initialized e.g., with $Q_w = 0$ (or $T_w = T_{bulk}$). The resulting flow temperatures and heat transfer coefficients are transferred to 3D solver (here ANSYS Fluent) after interpolation. There, the calculation is started with these boundary conditions, and it does not have to converge because the boundary conditions will be updated immediately by Flownex in the next global iteration. A suitable number of iterations in 3D Solver can be determined by trial and error. Afterwards, the old Q_w (or T_w) are replaced by the new values from the 3D calculation, which are used to generate new boundary conditions in Flownex for 3D model. In this way, the iteration continues until the alteration of the physical parameters is sufficiently small.

4. 1D, 3D and 1D/3D hybrid model

4.1 1D model of PSHX in Flownex

Flownex, like other 1D flow solvers, uses simplified conservation equations (conservation of mass, momentum and energy) to describe pressure drop, enthalpy change in a given flow element along one direction. While steady-state solutions are desired in this model, the model still can describe transient behaviour, which is one of the greatest advantages of 1D solvers.

The representation of the heat exchanger by 1D flow network model including heat transfer complements the previous prediction based on $\epsilon - NTU$ method with assumptions of constant material values, and prepares the 1D/3D coupled simulation. The heat exchanger segment can be modelled by the model shown in Fig. (7b). It comprises two flow elements ("hot" and "cold") and one heat transfer element ("Convection, main") between them. In addition to the main heat transfer through the partition wall, the air on the hot and cold sides are also thermally

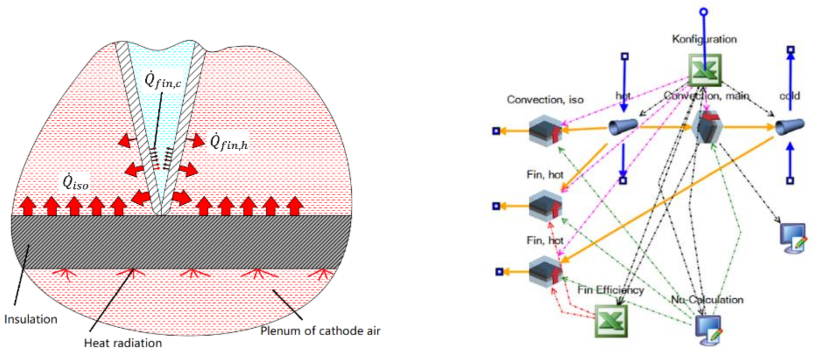

(a) Fin effects near the contact point between folded heating surface and insulation

(b) FNM of a heat exchanger segment

Figure 7: The fin effects and their representation in FNM

influenced by the insulation and the near-wall region of the partition wall (Fig. (7a)) also behaves like a fin due to the heat conduction in periphery. Consequently, three additional heat transfer elements ("Convection, iso", "Fin, hot", "Fin, cold") are connected to hot and cold side.

Flownex provides only standard elements, and therefore determining the triangular cross-sectioned duct's configuration is done on an Excel sheet. The corresponding flow area and periphery of the cross-section are then transferred to standard elements. The dependence of Nu on the geometry is realised through an implementation. The segment shown in fig. (8) is defined as a new component and marked by the corresponding connections, where the thicker dashed line stands for cold side, the thinner for hot side and the yellow and green for thermal connections to the 3D domain. The entire heat exchanger can be divided into several segments depending on resolution requirements. To determine the influence of the subdivision for an

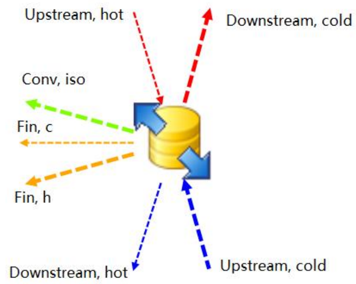

Figure 8: The custom-defined new compound in Flownex for a segment of heat exchanger

ideal heat exchanger (heat transfer through the partition wall), four different subdivisions were calculated for the comparison of the outlet temperature (table (5)). After the comparison, a subdivision of more than two sufficed. However, such behaviour (subdivision with two elements suffices) is expected, because there are similar $\dot{m}C_p$ on both sides of this heat exchanger. Thus, the temperature profiles on both sides are almost linear. If the $\dot{m}C_p$ on both sides were quite different, a fine subdivision might be necessary. 20 segments were eventually applied for 1D/3D hybrid model regarding possible non-linear temperature profile in the heat exchanger due to the influence of radiation.

Table 5: The influence of model discretisation on the outlet temperature of the cold side

Number of Discretization	1	2	10	20
Outlet temperature of cold side ($T_{c,o}$) in °C	688.24	700.64	700.61	700.61

4.2 1D/3D hybrid model for coupled simulation

4.2.1 Constitution of the hybrid model

The hybrid model assembly is based on continuous data exchange between different models. For the 3D part, a convection boundary condition is provided, in which the heat transfer coefficient and the flow temperature are delivered by the 1D model. For the 1D part, either the heat flux or the wall temperature extracted from the 3D model is required. The 3D part contains only the plenum and the insulation layer as shown in Fig. (9a), wherein one side of the insulation layer has been divided into twenty parts with respect to the subdivision of PSHX. For continuously varying temperature, the temperature profile was determined by piecewise linear interpolation:

$$T_{bulk} = T_{bulk,i} + \frac{T_{bulk,i+1} - T_{bulk,i}}{L_i}(z - z_i), z \in (z_i, z_{i+1}] \tag{11}$$

The heat transfer coefficients were set constant for a partial surface due to its slight change in the axial direction. A finer subdivision or interpolation schemes of higher order for more accuracy can also be used.

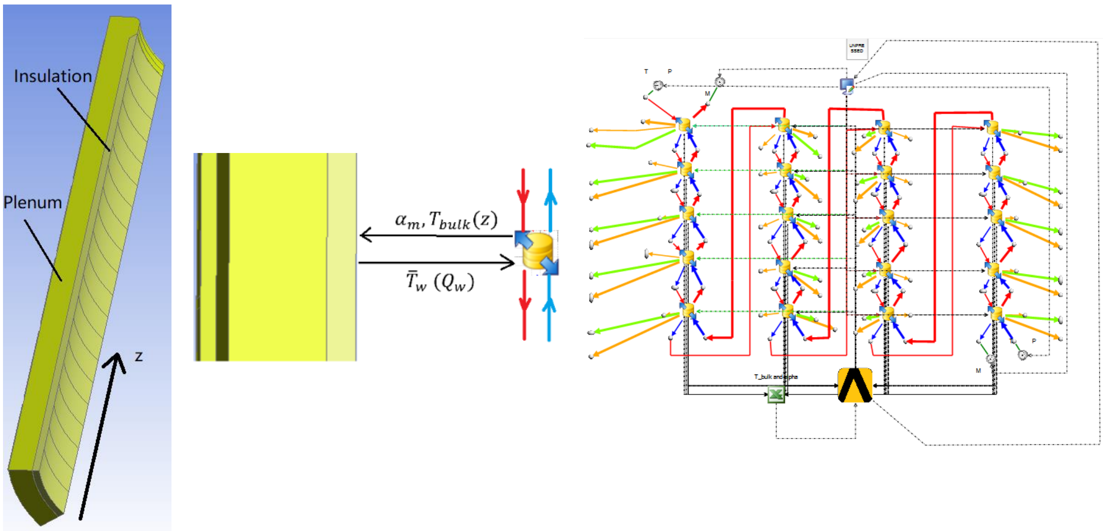

(a) Geometry of cathode exhaust air plenum and insulation

(b)Exchange of boundary conditions between 1D and 3D model

(c) 1D FNM of PSHX

Figure 9: Constitution of 1D/3D hybrid model

4.2.2 Numerical set up of 3D part of the hybrid model

The flow simulation including radiation in the plenum uses no turbulence model. The DO method [17] is employed for the radiation simulation. It was set up to calculate the radiation for every 10 iterations of the flow calculation. The working medium in this simulation (air) was treated as radiation permeable for simplicity. The emissivity of different materials was determined by an internal measurement. The temperature dependence of the thermal conductivity of the insulation layer is referred to data sheet of SILKAPAN 845. According to the grid study, 1.7 million grid elements with local refinement were used for meshing the plenum and the insulation layer. Mass flow and static temperature at the inlet (Fig. (10)) of the hot side were given as boundary conditions.

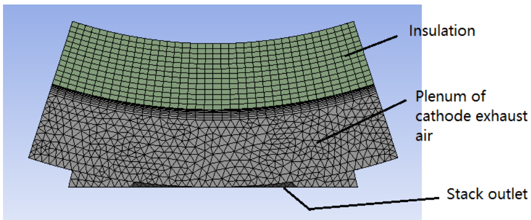

(a) Top view

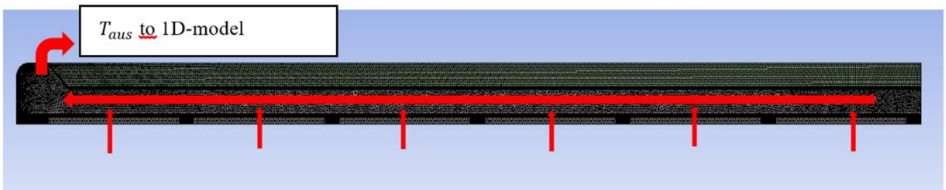

(b) Side view

Figure 10: Meshing of the 3D part of the hybrid model

4.3 3D model

4.3.1 3D model of the entire physical problem and of a single channel in PSHX

The entire 3D model and the corresponding meshing are shown in Fig. (11). Compared to the 1D/3D hybrid model, in a full 3D model the PSHX is also meshed and connected to the side of the plenum. The considered model represents for the reduction of the computational effort only one period of the full ring thanks to the periodic nature of the physical problem.

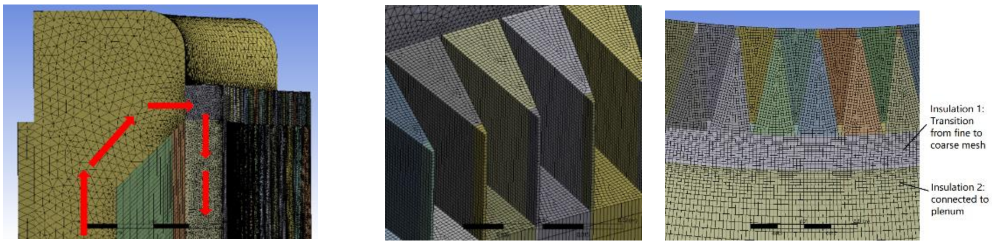

(a) Side view of the head region (b) Mesh at the junction (c) Mesh on the cross-section

Figure 11: Meshing of the 3D-CHT model

The channels in the PSHX require fine resolution and so a sum of approximately 15 million grid elements constituted the mesh. The apex of a single triangular channel is cut off for the benefit of the grid quality and provided with a straight edge. The grey ring-shaped zone shown in Fig. (11c) enables a milder transition between fine and coarse meshing, and better contact between the fluid and solid zones.

To validate the Nu used in the $\epsilon - NTU$ method and 1D model in Flownex, the smallest heat transfer unit of the PSHX is also simulated by 3D CFD, as shown in Fig. (12), which consists of two half channels of both sides. The partition wall between the cold and hot sides is modelled by shell conduction. According to the grid study, approximately 2.5 million elements are used for one channel.

(a) Geometry of a single channel (b) Meshing in the single channel

Figure 12: Meshing of a single channel PSHX

4.3.2 Numerical set up and boundary conditions

All simulations carried out in this work use no turbulence model, since laminar flow is simulated. The settings for the radiation simulation were presented in the previous section. A pressure-based solver is chosen for an incompressible flow. The material values of the air were made temperature dependent. The spatial discretization for pressure, momentum and energy are of second order, and a coupled scheme was used for pressure-velocity coupling.

5. Results and Discussion

5.1 Examination of the Nu-correlation and inclusion of the thermal entrance effects

The smallest heat transfer unit is simulated with 3D-CFD to verify the applied Nu-correlation, and the results are compared with those of $\epsilon - NTU$ and 1D model. A total of two configurations are calculated each with two different operating points. Table (6) lists the outlet temperatures of those cases. For all operating points, the inlet temperature of the cold side is set to 573.9 °C and of the hot side to 824.7 °C. The indicated mass flows refers to N pitches, which is 182 for IR and 432 for AR. According to Table (6), the 1D model reproduces the outlet temperature determined by $\epsilon - NTU$ with very small deviation because the PSHX designed in this work is operated with almost identical $\dot{m}C_p$ from both sides (so-called "balanced heat exchanger").

Table 6: Comparison among $\epsilon - NTU$, 1D and 3D CFD for single channel model

Config. 1 (IR)	P = 7.45 mm	OP-1 (IR): $\dot{m}_c$ = 0.127 kg/s	$T_{c,o}$ (°C)	$\epsilon - NTU$	698.03	$T_{h,o}$ (°C)	$\epsilon - NTU$	692.58
	H = 20 mm	$\dot{m}_h$ = 0.11 kg/s;		1D	700.27		1D	691.97
	s = 0.5 mm	$Re \approx 1500$		CFD	711.45		CFD	679.77
	L = 1497 mm			Mod. 1D	709.66		Mod. 1D	681.88
	D_m= 452 mm	OP-2 (IR): $\dot{m}_c$ = 0.0635 kg/s	$T_{c,o}$ (°C)	$\epsilon - NTU$	-	$T_{h,o}$ (°C)	$\epsilon - NTU$	-
		$\dot{m}_h$ = 0.055 kg/s;		1D	739.86		1D	649.14
		$Re \approx 800$		CFD	744.61		CFD	643.96
				Mod. 1D	747.71		Mod. 1D	640.58
Config. 2 (AR)	P = 11.5 mm	OP-1 (AR): $\dot{m}_c$ = 0.229 kg/s	$T_{c,o}$ (°C)	$\epsilon - NTU$	700.78	$T_{h,o}$ (°C)	$\epsilon - NTU$	690.63
	H = 20 mm	$\dot{m}_h$ = 0.213 kg/s;		1D	702.55		1D	689.51
	s = 0.5 mm	$Re \approx 1050$		CFD	711.57		CFD	679.91
	L = 1497 mm			Mod. 1D	711.91		Mod. 1D	679.47
	D_m= 1603 mm	OP-2 (AR): $\dot{m}_c$ = 0.1145 kg/s	$T_{c,o}$ (°C)	$\epsilon - NTU$	-	$T_{h,o}$ (°C)	$\epsilon - NTU$	-
		$\dot{m}_h$ = 0.107 kg/s;		1D	741.81		1D	647.01
		$Re \approx 500$		CFD	745.76		CFD	643.51
				Mod. 1D	749.55		Mod. 1D	638.56

In this case, besides thermal entrance effects, there is a nearly linear temperature distribution on both sides, for which the average temperature employed in the ϵ-NTU method to determine the material properties can satisfactorily account for the change in material properties along the heat exchanger. The observed deviation is mainly between the 1D and 3D single channel models, and becomes smaller with lower Reynolds number. The increased deviation between the 1D and 3D model indicates thermal entrance effects captured only in 3D simulation. These thermal entrance effects in the 1D model have been accounted by modifying the Nusselt number in the thermal entrance. This can be made dimensionless by the following equation [16]:

$$L_{hy}^{+} = \frac{L_{hy}}{d_h Re} \qquad (12)$$

where L_{hy} is the hydrodynamic entrance length and depends solely on the geometry for a laminar channel flow with triangular cross section [16]. For configuration 1, L_{hy}^{+} is about 0.045 corresponding to a hydrodynamic entrance length of about 400 mm at BP-1 (IR). Accordingly, Nusselt numbers of the first five segments (ca. 400 mm) in the 1D model were multiplied by a factor (>1), which decreases with increasing distance to the entrance of the respective side. The data for thermal entrance effects of a channel with equilateral triangular cross-section were evaluated for estimating magnification factors [16]. The magnification factors for the first five segments are presented in Table (7). Inclusion of the entrance effects makes deviations from the CFD results even smaller, especially for BP-1. Since a smaller Reynolds number namely a shorter entrance length occurs for BP-2, the magnification factors based on BP-1 give a slight overestimation of the exit temperature of the cold side compared to the CFD results. For the time being a further implementation for considering the dependence of the entrance length on Reynolds number is not made, because the achieved accuracy is satisfactory and the thermal entrance effects are marginal for heat exchangers operating in laminar condition with a ratio $\frac{L}{d_h}$ larger than 240.

Table 7: Magnification factors for the entrance effects

	Segment-1	Segment-2	Segment-3	Segment-4	Segment-5
Magnification Factor	3.0	2.6	2.2	1.6	1.2

5.2 Analysis of heat transfer mechanisms at the interface and adjustment of the 1D model

This section explains the heat transfer mechanisms at the junction between the PSHX and insulation layer. The comparison between the full 3D and 1D/3D hybrid simulation is meaningful only with proper representation of the heat transfer mechanisms on the contact surface. These local heat transfer mechanisms can be understood by plotting temperature contours as well as vectors of the heat flux on an axis normal cross-section intersecting the insulation layer and PSHX. In Fig. (13), as an example, the temperature contour and the local heat flux are shown using vectors of the temperature gradient. In the zoomed view of Fig. (13), a low temperature region at the contact point between the partition wall and the insulation layer can be recognized. The circumferential propagation of these regions leads to the formation of a so-called "sphere of influence". The formation of the "Low temperature region" indicates a local enhancement of the heat transfer due to

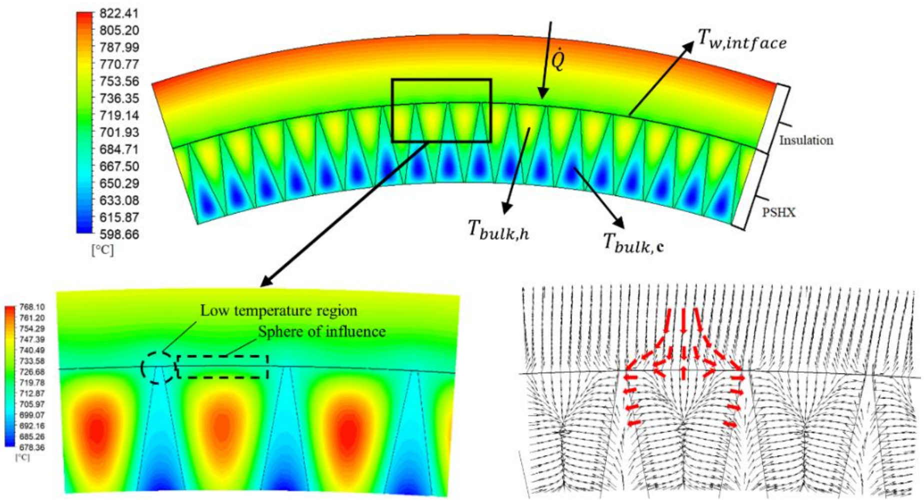

rib effects.

Figure 13: Illustration of heat transfer mechanism at the junction between insulation layer and PSHX

Observation on heat flux directions indicate that the heat conducted through the insulation layer has arrived exclusively in the cold side. The heat given off by the hot side is partly transported directly through the partition wall to the cold side and partly arrives indirectly on the cold side via the insulation layer.

The heat transfer enhancement caused by rib effects isn't suitable because it's a pure convective boundary condition for 3D part with the bulk temperature and heat transfer coefficient based only on the hot side. In the table (8), bulk temperatures of the cold and hot sides and a circumferentially averaged temperature on the interface are presented.

Table 8: Comparison between wall temperature, bulk temperature of both sides of PSHX

$T_{w,interface}$ (°C)	$T_{bulk,h}$ (°C)	$T_{bulk,c}$ (°C)
712.78	742.16	643.92

Table (8) indicates, the average temperature at the interface is lower than the bulk temperature of the hot side, which contradicts the previous approach, wherein the temperature on the interface must be greater than the bulk temperature of the hot side to ensure the direction of heat flux (from plenum of cathode exhaust air towards PSHX). Contextually, three adaptation procedures are adopted to account for these mechanisms in the 1D/3D coupling:

- Heat flow through the insulation layer enters the cold side only by disabling the heat transfer elements connected to the hot side in the figure (7b). The amount of heat transferred indirectly from the hot side to the cold side is considered, if necessary, by increasing the heating surface between the hot and cold sides.
- Introduction of modified bulk temperature as a boundary condition for the 3D model:

$$T_{bulk,equ} = \phi T_{bulk,h} + (1-\phi) T_{bulk,c} \tag{13}$$

where ϕ varies between 0 and 1. Introducing the parameter ϕ helps consider the influence of the cold side on the bulk temperature felt by the insulation layer. A value of 1 describes the case where heat is transferred entirely to the hot side by convection leading to an underestimation of the total amount of transferred heat. A value of 0 indicates convection only with the cold side resulting in an overestimation of the amount of heat transferred.

- Enlarging the heating surface between hot and cold side to the whole periphery of a triangular cross-section

5.3 Comparison between full 3D-CHT and 1D/3D hybrid simulation

5.3.1 Comparison at different insulation thickness for full load

This section compares full 3D-CHT and 1D/3D hybrid simulation based on findings in section 5.1 and 5.2. The simulations performed for comparison and calibration are based on configuration 1 and BP-1 in Table (6). Fig. (14) presents the comparison of temperature distribution between full 3D-CHT and 1D/3D-hybrid simulation. Three different insulation thicknesses are considered, 34 mm, 17 mm and 5 mm. The parameter ϕ is varied between 0.1 and 0.7 with an interval of 0.2. For all considered ϕ, only small variations are observed for insulation thicknesses of 34 mm and 17 mm. At 5 mm insulation thickness, an increased deviation is observed mainly at the outlet of the respective side of the PSHX, and it decreases with reducing ϕ, especially for the cold side. A maximum deviation occurring at the exit of the hot side is within 10 percent. Also deducible is an increasing influence of the ϕ on the temperature distribution with decreasing insulation thickness. This is justifiable by the fact that the thermal resistance in thick insulation is dominated by insulation's thermal conduction, such that a change in convection, with comparatively smaller thermal resistance to thermal conduction in the insulation, has less influence on total resistance. In the case of thinner insulations, ϕ exerts more influence because it influences the thermal resistance in convection, as it is the case in Fig. (14).

Table 9: Comparison of total amount of heat transferred through the insulation layer for different simulation methods at full load

Total heat transfer through the insulation in W (for 1 period)	34 mm (with $\phi = 0.1$)	1D/3D hybrid simulation	293.43
		full 3D-CHT	241.27
	17 mm (with $\phi = 0.1$)	1D/3D hybrid simulation	427.72
		full 3D-CHT	403.49
	5 mm (with $\phi = 0.1$)	1D/3D hybrid simulation	677.90
		1D/3D hybrid simulation (cali)	887.19
		full 3D-CHT	811.65

Table (9) shows the amount of heat transferred through the insulation (for one period) for different insulation thicknesses. Like the temperature distribution, increased deviation is noticeable for the insulation thickness of 5 mm. One reason for the larger difference between fully 3D-CHT and 1D/3D hybrid simulation at smaller insulation thickness would be the inability of the pure convection boundary condition assumption for the 3D part of the hybrid simulation to fully represent the heat transfer mechanisms at the contact point. Another reason is stronger cooling of the cathode exhaust air due to overestimation of the effective heating area between the cold and hot sides in the 1D model of the PSHX. There are two possible improvement measures to counteract the increasing deviation with thinner insulation thickness. The first is to artificially increase the heat transfer coefficients to be transferred from 1D to 3D model to allow for more heat flow through the insulation with an expected increase of the outlet temperature at both sides. Thus, the cold side experiences a greater temperature increase than the hot side because of the direct heat transfer from 3D simulation to cold side of 1D model. The second is, reducing the heating area between the cold side and hot side in 1D model. With this measure, the cold and hot sides experience similar temperature change. Based on these findings, the 1D/3D hybrid model for 5 mm insulation thickness is additionally calibrated by adjusting the heat transfer coefficients so that the overestimation of the cold side has similar magnitude as the underestimation of the hot side, and the heating area is reduced until the overestimation and underestimation of both sides are sufficiently small. After the calibration, a clear improvement identified as shown in Fig. (14) and Table (9).

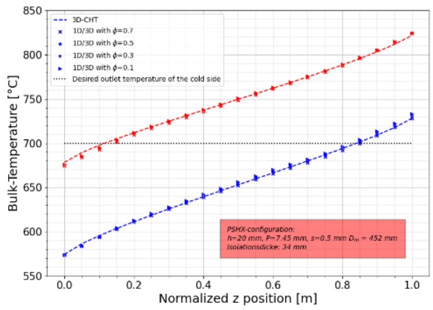

(a) 34 mm

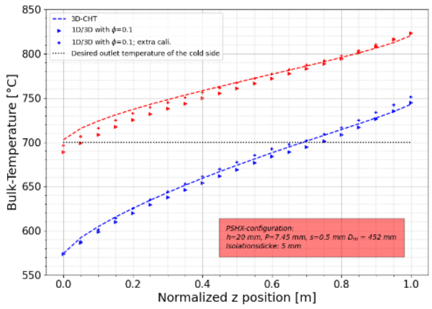

(b) 17 mm

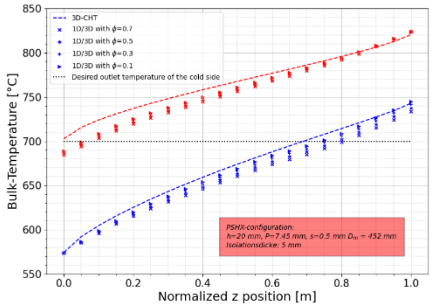

(c) 5 mm

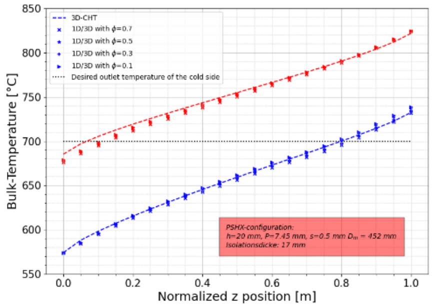

(d) 5 mm with extra calibration

Figure 14: Comparison of temperature distribution (red: hot side, blue: cold side) between 3D-CHT und 1D/3D hybrid simulation for different thickness of insulation layer at full load

5.3.2 Comparison at different insulation thickness for partial load

The simulation results, with the same settings, are also compared at partial load (BP-2) as shown in Table (10). The comparison reports a slight overestimation of the outlet temperature of the cold side by about 5 to 10 °C (about 5 percent) with 1D/3D hybrid model, while a significant underestimation of about 15 to 30 °C (about 20 percent) appears on the hot side. With the previously recommended adjustment measures of the 1D model at 5 mm insulation thickness, the deviation compared to 3D-CHT is reduced to a lower level.

In addition to the predicted temperature, the amount of heat transferred through the insulation layer was also compared. In this comparison, the deviations from full 3D-CHT are very small, thereby proving the validity of the 1D/3D hybrid model even at partial load.

Table 10: Comparison of total amount of heat transferred through the insulation layer for different simulation methods at partial load

Total heat transfer through the insulation in W (for 1 period)	34 mm (With ϕ = 0.1)	1D/3D hybrid simulation	226.86
		Full 3D-CHT	241.27
	17 mm (With $\phi = 0.1$)	1D/3D hybrid simulation	356.38
		Full 3D-CHT	368.08
	5 mm (With $\phi = 0.1$)	1D/3D hybrid simulation	526.83
		1D/3D hybrid simulation (cali.)	663.49
		Full 3D-CHT	663.14

Table 11: Comparison of the outlet temperature of both sides of PSHX for different simulation methods at partial load

34 mm	$T_{c,o}$ (°C)	3D-CHT	769.66
		1D/3D hybrid simulation	774.98
	$T_{h,o}$ (°C)	3D-CHT	660.52
		1D/3D hybrid simulation	645.40
17 mm	$T_{c,o}$ (°C)	3D-CHT	773.27
		1D/3D hybrid simulation	782.44
	$T_{h,o}$ (°C)	3D-CHT	667.80
		1D/3D hybrid simulation	651.67
5 mm	$T_{c,o}$ (°C)	3D-CHT	787.28
		1D/3D hybrid simulation	791.30
		1D/3D hybrid simulation (cali.)	798.24
	$T_{h,o}$ (°C)	3D-CHT	693.87
		1D/3D hybrid simulation	665.60
		1D/3D hybrid simulation (cali.)	677.35

5.3.3 Influence of PSHX configuration on the comparison

Simulations were performed for two other PSHX configurations (Table (12)) to examine the accuracy of the prediction from the 1D/3D hybrid model for new PSHX configurations. Here, the pitch count is set to N = 160 and N = 140. All other parameters such as mean diameter (D_m), channel height, boundary conditions, etc. remain identical as in section 5.3.1. Results from the Table (12) claim, that the 1D/3D hybrid model can deliver results comparable to 3D-CHT even for the new PSHX configuration. The insensitivity of the total heat transferred through the insulation to pitch count can also be reproduced with the 1D/3D hybrid model.

Table 12: Comparison for different PSHX configurations at full load and insulation layer thickness of 34 mm

N	$T_{c,o}$ (°C)		$T_{h,o}$ (°C)		Total heat transfer through the insulation in W	
	1D/3D	3D-CHT	1D/3D	3D-CHT	1D/3D	3D-CHT
180	733.08	728.02	676.35	678.46	293.43	241.27

160	721.70	720.01	688.60	686.90	293.84	240.94
140	710.04	710.69	701.18	697.20	294.05	235.23

5.3.4 Comparison of computing efforts

HPC (High Performance Computing) is used to calculate 3D-CHT, while only one PC was used for 1D/3D hybrid simulation. The total computation time for one simulation of 3D-CHT is about 12 hours with over 100 CPUs in the computational cluster. For the 1D/3D hybrid simulation, the computation time is about 2 hours on average with 10 CPUs in use. The savings in computing time and computing resources are significant. Considering the comparison results between the two methods, the well-calibrated 1D/3D hybrid model is an alternative to the fully 3D-CHT.

5.4 Behaviour of the PSHX under the influence of thermal radiation and development of further design strategies

The thermal radiation influence assessment considers the plot of the temperature distributions of all three insulation thickness together with the reference case, as in Fig (15).

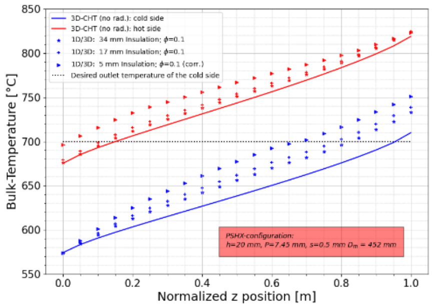

Figure 15: Comparison of temperature distribution under influence of heat radiation at different insulation thickness

The Figure (15) shows that thermal radiation has more influence on the cold side. At 5 mm insulation thickness there is an additional temperature increase of more than 40 °C at the cold side exit, while at the hot side exit it is only about 20 °C. The difference, graphically illustrated in Fig. (13) is due to heat transfer mechanisms at the contact surface. As mentioned in previous sections, the heat transfer mechanism at the contact surface differs from that of pure convection regard to heat conduction effects through the ribs. With the help of the ribs, the heat that should be collected entirely from the hot side, if there were no contact between the partition wall and the insulation layer, is transported directly to the cold side and subsequently warms up the fresh incoming air. If heat exchanger’s effectiveness is evaluated according to its original definition (Eq. (2), an increase in effectiveness is obtained, as shown in Table (13). A larger increase in effectiveness can be seen at partial load. The increase in effectiveness is due to the additional heat input into the cold side because of the fin effects. It should be noted that the effectiveness in this case can be greater than one, because the provided heat radiation is independent of the maximum exchangeable amount of heat, which depends exclusively on inlet temperatures at both sides of the heat exchanger.

Table 13: Comparison of heat exchanger effectiveness for different thickness of insulation layers

	Effectiveness: ϵ	
	BP-1	BP-2
Ref. Cases (Without Radiation, config. 1)	0.57 (DP)	0.72
34 mm	0.64	0.82
17 mm	0.66	0.83
5 mm	0.70	0.88

From these discussions, the following design strategies are suggested. Firstly, reducing the number of pitches to avoid the temperature overshooting (over-design). Secondly, adjusting the allowed thermal radiation in favor of cooling the stack by varying the pitch number and insulation thickness, without changing the outlet temperature of the cold side. Thus, the second strategy incorporates thermal load shifting between internal heat transfer of the heat exchanger and external heat input. Thirdly, variation of the insulation thickness so that PSHX of IR and AR has the same configuration (same pitch width) benefiting the series production of the profiled sheet in the future.

6 Conclusion and outlook

In this work, initially a PSHX based on $\epsilon - NTU$ theory is pre-designed, which is used as a key component to realize the MGT-SOFC hybrid process. In anticipation of complicated analysis, the next step involved modelling the PSHX by a 1D FNM. The behaviour of this PSHX under the influence of thermal radiation from the stack module was understood through the co-simulation method to simulate the radiation by 3D simulation and model the PSHX by 1D FNM. The validity of the 1D/3D hybrid model was verified by creating a complete 3D-CHT model and performing the corresponding simulations. The comparison between the two methods indicates, that the fitted 1D/3D hybrid model with its low computational costs and short computational time is an attractive alternative to the 3D-CHT simulation. The behaviour of the PSHX was discussed with obtained results. The stronger influence on the cold side of the PSHX due to fin effects and an increase in effectiveness were observable. In conclusion, three design strategies were developed, which were not further discussed in detail because their discussion is outside the scope of this paper:

1. Reduction of Pitch number to avoid temperature overshooting at the cold side outlet
2. Targeted determination of insulation thickness and PSHX-configuration depending on the cooling requirements (heat transfer through radiation) of the stack module
3. Targeted determination of insulation thickness so that the same PSHX-configuration for both IR and AR could be used for the benefit of mass production of profiled metal sheet

In the next step, the 1D/3D model developed in this work will be validated and calibrated with experimental data, the acquisition of which is currently in progress. In parallel, the dynamic model of the stack module with different complexities (0D/1D/3D) will also be developed, which will later be coupled with the 1D/3D model developed in this work to capture the interaction between stack module and PSHX and prepare for transient and dynamic analysis.

References

[1] H.P. Berg, A. Himmelberg, M. Lehmann, R. Dückershoff and M. Neumann (2017). *The Turbo-Fuel-Cell 1.0 – family concept*. 8th TSME-International Conference on Mechanical Engineering (TSME-ICoME).

[2] H. P. Berg, R. Dückershoff, A. Himmelberg and U. Ring (2021). *Simulations using dimensionless key figures for the design and optimization of compact, hybrid MGT-SOFC systems of the "TURBO FUEL CELL" type for high efficiency*. 14th European Conference on Turbomachinery Fluiddynamics & Thermodynamics.

[3] Prof. Dr.-Ing. Hein Peter Berg and Dipl.-Ing. Christian Krienke (2015). *Mikrogasturbinen-SOFC-Prozesse mit hohem Wirkungsgradpotential*. 12. Magdeburger Maschinenbau-Tage.

[4] W. M. Kays, A. L. London (1964). *COMPACT HEAT EXCHANGERS*. United States of America, McGRAW-HILL BOOK COMPANY.

[5] Norihiko Watanabe, Masahiko Kubo, Nobuyuki Yomoda (2006). *An 1D-3D Integrating Numerical Simulation for Engine Cooling Problem*. SAE World Congress, Detroit Michigan.

[6] Haimi Jordaan, P. Stephan Heyns, Siamak Hoseinzadeh (2021). *Numerical Development of a Coupled One-Dimensional/Three-Dimensional Computational Fluid Dynamics Method for Thermal Analysis With Flow*

Maldistribution. Journal of Thermal Science and Engineering Application, Vol. 13/041017-1, DOI: 10.1115/1.4049040.

[7] W. Puntigam, T. Hörmann, K. Schierl, B. Wieler and J. Hager (2005). *Thermal Management Simulations by Coupling of Different Software Packages to a Comprehensive System*. Vehicle Thermal Management Systems Conference and Exhibition, Toronto Canada.

[8] Pengyu Lu, Qing Gao, Yan Wang (2016). *The Simulation methods based on 1D/3D collaborative computing for the vehicle integrated thermal management*. Applied Thermal Engineering, 104(2016)42-53, https://doi.org/10.1016/j.applthermaleng.2016.05.047.

[9] Vivek Kumar, Sangeet Kapoor, Gyan Arora, Sandip K. Saha and Pradip Dutta (2009). *A Combined CFD and Flow Network Modeling Approach for Vehcle Underhood Air Flow and Thermal Analysis*. SAE International, DOI: 10.4271/2009-01-1150.

[10] Peter Grafenberger, Pascal Klinner, Peter Nefischer, Felix Klingebiel (2000). *Simulation der Motorkühlung mit Hilfe gekoppelter 1D- und 3D-Strömungsberechnung*. ATZ Automobiltechnische Zeitschrift, DOI: 10.1007/bf03221545.

[11] Pol Reddy Kukutla, B.V.S.S.S Prasad (2017). *Coupled Flow Network Model and CFD Analysis for a Combined Impingement and Film Cooled Gas Turbine Nozzle Guide Vane*. AMSE JOURNALS-AMSE IIETA, pp 250-270, DOI: 10.18280/mmc_b.860118.

[12] Tom Kowalski, Amir Radmehr (2000). *Thermal Analysis of an Electronics Enclosure: Coupling Flow Network Modeling (FNM) and Computational Fluid Dynamics (CFD)*. Annual IEEE Semiconductor Thermal Measurement and Management Symposium, DOI: 10.1109/STHERM.2000.837062.

[13] K. Höschler, J. Bischof, W.Koschel (2000). *THERMO-MECHANICAL ANALYSIS OF AN AUTOMOTIVE DIESEL ENGINE EXHAUST MANIFOLD*. European Structural Integrity Society, Volume 29, 2002, Pages 299-308, https://doi.org/10.1016/S1566-1369(02)80086-3

[14] Theodore L. Bergman, Adrienne S. Lavine, Frank P. Incropera and David P. Dewitt (2011). *Fundmentals of Heat and Mass Transfer*. United States of America, JOHN WILEY & SONS.

[15] Richard C. Cope and Richard W. Hanks (1972). *Transitional Flow in Isosceles Triangular Ducts*. Industrial and Engineering Chemistry Fundamentals, Vol. 11, No. 1, 1972. DOI: 10.1021/i160041a016.

[16] R. K. Shah, A. L. London (1978). *LAMINAR FLOW FORCED CONVECTION IN DUCTS*. United States of America, ACADEMIC PRESS

[17] *ANSYS Fluent Theory Guide*. ANSYS, Inc.